DOI: 10.1002/ejoc.200800762

DFT/MM Study on Copper-Catalyzed Cyclopropanation – Enantioselectivity with No Enthalpy Barrier

Galí Drudis-Solé,[a,b] Feliu Maseras,*[a,b] Agustí Lledós,[b] Adelina Vallribera,[b] and Marcial Moreno-Mañas[b][‡]

Keywords: Density functional calculations / Enantioselectivity / Cyclopropanation / Copper / Carbene ligands

The enantioselectivity in the reaction of [Cu(adam-box)(CHCO$_2$Me)] {adam-box = 2,2′-isopropylidenebis[(*4R*)-(1-adamantyl)-2-oxazoline]} with $Ph_2C{=}CH_2$ was analyzed computationally by ONIOM(B3LYP:UFF) calculations. The lack of transition states in the potential-energy surface precludes the use of conventional approaches and requires the definition of reaction paths in an approximate Gibbs free-energy surface. The procedure is time consuming and intrinsically less accurate than the usual approaches based on enthalpic energy surfaces, but it produces results in reasonable agreement with experiment, which furthermore allow identification of the key interactions responsible for chiral discrimination.

(© Wiley-VCH Verlag GmbH & Co. KGaA, 69451 Weinheim, Germany, 2008)

Introduction

The cyclopropane ring is an important unit in organic chemistry.[1–4] It is present in a number of relevant compounds,[5–7] it produces unusual structures,[8–10] and it is part of many versatile synthetic intermediates.[11,12] Substituted cyclopropane rings are potentially chiral, and their enantioselective synthesis has been the subject of intense research in recent years.[13–18] The reaction of diazoalkanes with olefins catalyzed by transition-metal complexes (Scheme 1) is among the most used techniques for stereoselective preparation of cyclopropane species.

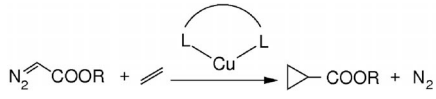

Scheme 1. Cyclopropanation of olefins by copper catalysts.

The decomposition of the diazo species is catalyzed by a variety of transition-metal complexes, but among them, copper species with bis(oxazoline) ligands (Figure 1) have been found to be particularly useful.[19–28] Their widespread use is associated with the ease with which C_2 enantiopure ligands derived from malonic acid can be accessed.[29,30] In particular, some of us have been able to synthesize the 2,2′-isopropylidenebis[(4*R*)-(1-adamantyl)2-oxazoline] ligand (adam-box) ligand, with adamantyl substituents.[31–33] The Cu[adam-box] complex performs excellently in cyclopropanation, Diels–Alder, and allylic oxidation processes.[31] In particular, the catalysis of the reaction of ethyl diazoacetate (EDA) with 1,1-diphenylethylene accomplishes cyclopropanation with an enantiomeric excess of over 95%.

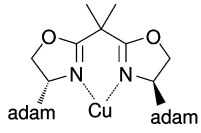

Figure 1. [Cu{bis(oxazoline)}] C_2 complex.

Computational chemistry has been used extensively in recent years for the clarification of reaction mechanisms in homogeneous catalysis.[34] In particular, density functional theory/molecular mechanics (DFT/MM) methods have been successfully applied by us and others to a number of enantio- and regioselective processes.[35–39] It seems thus appropriate to apply this same approach to the study of the origin of enantioselectivity in this particular system.

Previous computational studies on the cyclopropanation reaction catalyzed by metal complexes have led to the characterization of the general mechanism shown in Scheme 2.[40–49] In the first steps, the diazo derivative coordinates to the metal center and diatomic nitrogen is extruded, which results in a complex where the reactive carbene is coordinated to the copper center. The elimination of dinitrogen is the rate-determining step of the overall process. The carbene complex reacts then with the olefin to form the cyclopropane ring. Afterwards, the reaction prod-

[a] Institute of Chemical Research of Catalonia (ICIQ),
Av. Països Catalans 16, 43007 Tarragona, Catalonia, Spain
Fax: +34-977-920-0231
E-mail: fmaseras@iciq.es
[b] Departament de Química, Edifici Cn, Universitat Autònoma de Barcelona,
08193 Bellaterra, Catalonia, Spain
[‡] Deceased: February 20, 2006.

 WILEY InterScience DISCOVER SOMETHING GREAT © 2008 Wiley-VCH Verlag GmbH & Co. KGaA, Weinheim

uct remains weakly attached to the metal center through the oxygen atom of a carbonyl group, and the final step is dissociation of the product and regeneration of the catalyst. The reaction between the carbene and the olefin is the step where the enantioselectivity of the process is decided. All bonds in the cyclopropane are formed here, and they are not broken afterwards. Therefore, the configuration of the product is defined at this point.

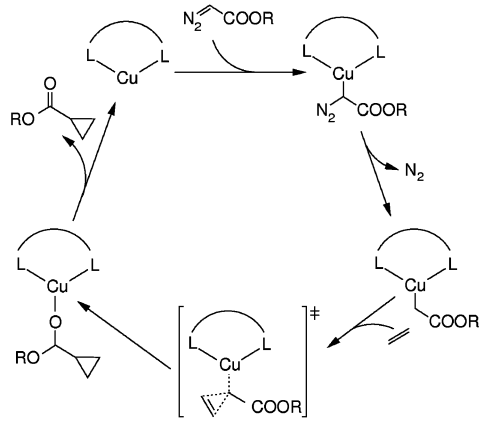

Scheme 2. Proposed mechanism for the cyclopropanation reaction.

The origin of enantioselectivity can thus be analyzed with a study of the particular step where the olefin binds to the carbene. The topic has been indeed successfully analyzed in ruthenium complexes by García and coworkers[45,46] in the usual terms of comparing the barriers for the transition states leading to the *R* and *S* products. Unfortunately, the topic is seriously complicated for copper species by the absence of an enthalpic barrier to the process, at least for some particular cases. The entropy control of some carbene cycloadditions was already identified by Houk and Rodan in 1984[50] and has been further confirmed for the particular case of copper carbene species by Norrby and coworkers in 2002.[40] This poses a serious problem to the analysis of enantioselectivity. The conventional approach of computing the transition state in the potential-energy surface is no longer valid, because there is a smooth descent from the separated fragments to the product where the cyclopropane is already formed. There is, however, a barrier in free energy, and our goal in this paper is to see if we can estimate it with simple computational approaches to gain insight into the enantioselectivity of the overall process.

Results and Discussion

Enthalpy Barrier versus Gibbs Free-Energy Barrier – Synchronicity

The absence of a transition state in the potential-energy surface[40] invalidates the conventional approximations based on the location of a transition state on the potential-energy surface and the estimation of its free energy from single-point calculations on this structure. No analytic gradients for Gibbs free energy are available in the usual computational packages, and location of the transition state thus has to be approached through numerical calculations of a minimum energy path in the corresponding surface. This approach requires careful selection of the least number of coordinates that can describe the reaction advance so that the dimension of the surface does not make the calculations unaffordable. In our case, only two coordinates suffice: the distances from each of the carbon atoms of the reacting olefin to the carbene, d_1 and d_2.

The surfaces for Gibbs free energy and potential energy were studied in a model system to evaluate the synchronicity of the reaction. The model system consists of [Cu(NH–CH–CH_2–CH–NH)($CHCO_2Me$)] plus CH_2=CH_2. The axes of the surface are x and y, and they are defined from the distances d_1 and d_2 as $x = (d_1 + d_2)/2$ and $y = (d_1 – d_2)/2$. The choice of x and y is based on chemical criteria. The x variable, which is the average of the distances between the olefinic carbon atoms and the carbene, carries the information of the degree of advance of the reaction, whereas the y coordinate reveals how similar these distances are, that is, the synchronicity. Having small values of y for the minimum energy path implies high synchronicity, that is, both bonds are formed almost at once, whereas large values of y imply that the formation of the bonds of the cyclopropane is stepwise, that is, one is formed after the other.

The resulting potential-energy surface is shown in Figure 2. Its general shape confirms the previously documented absence of a transition state. There is a smooth descent of energy from the separate reactants (large x) towards the product (small x). From the point of view of synchronicity, the path with $y = 0$ coincides with the minimum energy path. This means that taking into account only the potential energy, the reaction will be synchronic. The free-energy surface is presented in Figure 3. Here, the energy of most of the surface is higher than that of the reactants; therefore, there exists a transition state in the Gibbs free-energy surface. For the model system used, the transition state is lo-

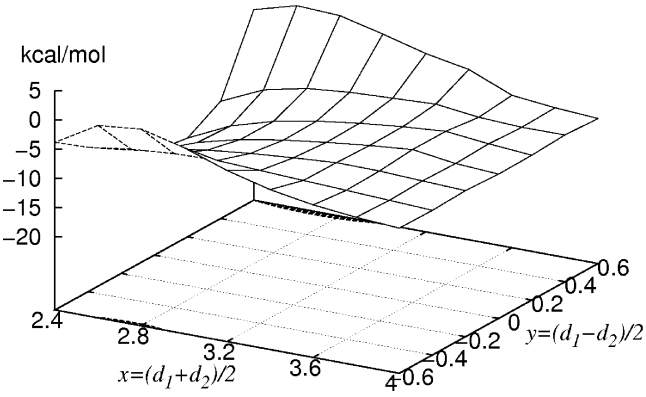

Figure 2. Potential-energy surface in the region where the transition state is expected. Only contours with energies above that of the reactants are printed.

 © 2008 Wiley-VCH Verlag GmbH & Co. KGaA, Weinheim

cated at x = 3.6 Å, y = 0.0 Å, and ΔG = 5.7 kcal/mol above the reactants. This low barrier agrees with a fast reaction occurring at room temperature and below. A straightforward conversion from x and y to d_1 and d_2 yields d_1 = 3.6 and d_2 = 3.6 for the transition state. The synchronicity of the potential-energy surface is conserved for the Gibbs free-energy surface, as both olefinic carbon atoms approach simultaneously to the carbene. A closer inspection of Figure 3 reveals that synchronicity is near perfect for olefin–carbene mean distances of 3.6 Å and below, whereas above this distance, the surface becomes more flat, and different paths of similar energy become accessible.

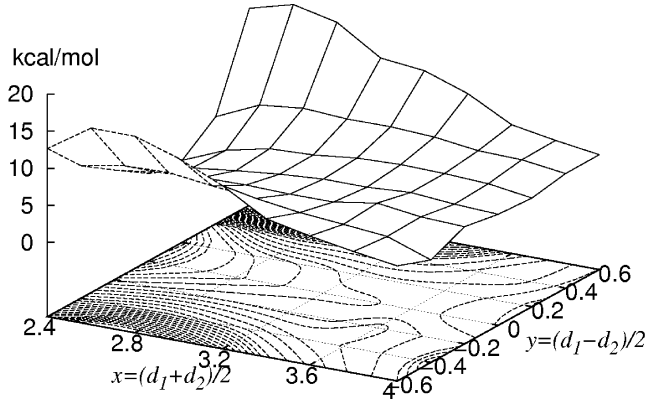

Figure 3. Approximate Gibbs free-energy surface in the region where the transition state is expected. Only contours with energies above that of the reactants are printed. Different contour lines correspond to a Gibbs free-energy difference of 0.5 kcal/mol.

The introduction of the steric and electronic effects of the real system will surely include some asynchronicity between the two olefinic carbon atoms. However, the use of a synchronous pathway allows the computational effort required to be reduced by more than an order of magnitude and is likely to provide still a reasonable estimation.

Twenty-Four Possible Reaction Paths

The calculation of enantioselectivity requires the calculation of the reaction paths going to the *R* and *S* products and comparison of their barriers. The choice of these paths is not straightforward, and several possibilities have to be systematically analyzed.

The reaction step under study consists of the approach between two fragments, the copper carbene complex and the olefin. The structure of the olefin, 1,1′-diphenylethylene, is straightforward, but the structure of the carbene deserves some discussion. Figure 4 presents its optimized structure. The carbenic center C_{carb} is in a trigonal arrangement, and its three substituents, Cu, H, and C, are coplanar. Rotation around the Cu–C_{carb} axis is, however, essentially free. Orientation of this plane is critical for the reaction path, because the olefin will approach in a direction perpendicular to it. Consequently, the possible orientations of this plane have to be considered. Our study shows that three different orientations must be taken into account, those labeled as A, B, and C in Figure 5.

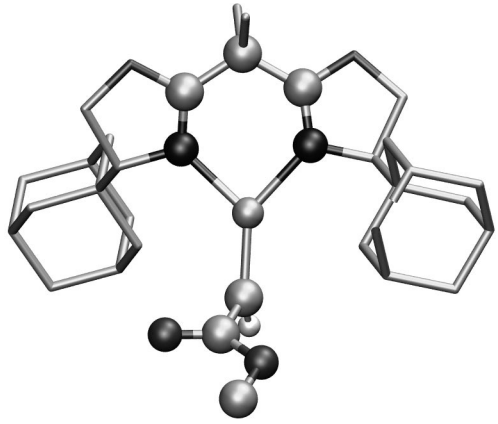

Figure 4. Structure of the intermediate; hydrogen atoms not attached to the carbene are removed for clarity.

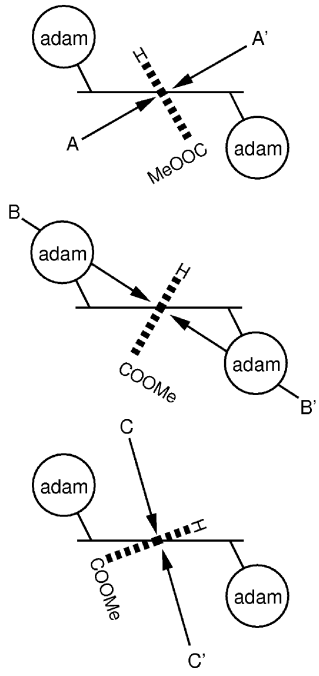

Figure 5. Approach paths of diphenylethylene to the carbene. The molecule is viewed from the Cu–carbene axis; the carbene is at the back of the Figure and the bis(oxazoline) ring is at the top.

In directions A and B, the carbene plane stays essentially perpendicular to the N–Cu–N bis(oxazoline) plane, and this is the favored arrangement of the intermediate species. The carbene is slightly tilted with respect to the perpendicular, which allows the entering olefin to avoid the bis(oxazoline) plane. Directions A and B differ in the direction of the tilt: the tilt is towards the adamantyl substituents in direction A and opposite to them in direction B. The schematic drawing in Figure 5 shows that in direction B the olefin must pass below the adamantyl groups, and therefore, an additional direction C was considered, where the carbene

 © 2008 Wiley-VCH Verlag GmbH & Co. KGaA, Weinheim

plane is nearly eclipsed with the oxazoline plane; this allows the olefin to enter near the perpendicular direction. A hypothetical path D, in which the carbenic plane eclipses the adamantyl groups, was found to be impossible in test calculations because of its high steric strain.

Directions A, B, and C give rise to two paths each, labeled arbitrarily as A, A′, B, B′, and C, C′, depending on the face where the approach to the carbene plane takes place. These faces are not equivalent, because one side of the oxazoline contains the ester group and the other does not, as shown in Figure 5.

A second source of path diversity is in the relative positions of the oxy and methoxy substituents of the carbon atom attached to the carbene. It can be seen in Figure 4 that there is no conjugation between the π systems of the carbene and carboxyl systems, which are nearly perpendicular. This type of arrangement is not unexpected, as it was already reported in DFT calculations of other transition-metal carbene complexes.[45,51] It has, in any case, the important consequence of adding conformational complexity to the system and duplicates the available paths previously shown in Figure 5. We will discriminate between these two set of paths by adding a new label, + or –, depending on the sign of the Cu–CH–C=O dihedral angle.

The last source of complexity comes from the substitution pattern of the olefin. One carbon atom has two hydrogen atoms and the other has two phenyl groups attached. The relative position of the substituents with respect to the carbene will decide finally the stereoselectivity of the cyclopropane product, and because of this, we will use directly the *R* and *S* labels to discriminate these paths.

In summary, we have defined three labels for each path, depending on the attack direction (A, B, C, A′, B′, or C′), the sign of the Cu–C–C=O dihedral angle (+ or –), and the stereoselectivity of the product formed (*R* or *S*). The nomenclature used hereafter will make use of these labels in the form "DsE", where D is the information regarding the attack direction, s is the sign of the dihedral angle, and E is the enantiomer formed. As each of the three variables is independent of each other, the number of possible paths is 24 ($6 \times 2 \times 2$), all of which will have to be studied.

Computed Enantioselectivity

After having defined the reactive paths, the next step is to study the Gibbs free-energy profile for each of them. The computational cost of building full surfaces is prohibitive, and we have concentrated on synchronic paths with identical values for the two C–C bonds being formed. The step used was 0.2 Å. This provided us with 24 Gibbs free-energy profiles, from which we found the points of maximum energy of each profile. These values were used as an estimation of the position and energy of the point of maximum energy in the Gibbs free-energy surface for each reaction path.

The results corresponding to the maximum energy point in each profile are summarized in Table 1. The Table includes also the proportion of final product emerging from each path obtained from the relative energies of these maximum energy points. Data are given to the tenth of a percentage point to emphasize differences between the least-favored paths, although we do not claim such a high accuracy for our calculations. Similarly, we made the transformation of energy differences to product proportions for the sake of clarity, although we are aware that our calculations are not that accurate. The addition of all the reactive paths leading to the *R* and *S* enantiomers leads to the prediction of 95% *S* enantiomer and 5% *R* enantiomer. This represents a computed enantiomeric excess in favor of the *S* product of 90%, which is not as high as the experimental observation of 98%, but the value is in very reasonable agreement.

Table 1. Summary of results for the highest Gibbs free-energy point in each of the computed paths. Data provided are the C_{carb}–C_{olefin} distances (*d*, Å), Gibbs free energies above the reactants (*G*, kcal/mol), and percent of the reactions occurring through each path at 298 K [%].

	S			*R*		
	d	Δ*G*	%	*d*	Δ*G*	%
A+	3.2	12.4	0.0	2.6	20.2	0.0
B+	2.8	8.9	1.0	–	–	–
C+	3.2	8.7	1.3	2.7	14.1	0.0
A–	2.8	11.1	0.0	3.2	14.2	0.0
B–	3.2	8.4	2.4	–	–	–
C–	3.2	6.3	88.	2.6	14.1	0.0
A′+	3.4	9.1	0.8	4.2	7.9	5.1
B′+	–	–	–	3.0	13.9	0.0
C′+	4.0	13.4	0.0	3.6	16.1	0.0
A′–	3.2	11.6	0.0	2.8	11.9	0.0
B′–	–	–	–	2.6	15.8	0.0
C′–	4.2	8.7	1.4	2.8	16.5	0.0

The data from some of the proposed paths are absent from Table 1. These are B′+*S*, B′–*S*, B+*R*, and B–*R*. The calculations starting from any of these paths ended in one of the other possible paths. All these paths correspond to the B direction, and they collapse in the related paths in the C direction. As previously shown in Figure 5, directions B and C differ only in the degree of torsion around the Cu–C_{carb} axis, and path B corresponds to the case where the olefin enters close to the adamantyl groups. As a result, in the paths where the bulky phenyl substituents of the olefin are far from the adamantyl moiety, no differentiated path corresponding to the B direction exists.

Comparison between directions A and C is also informative. Direction A represents the carbene orientation preferred in the isolated intermediate, whereas direction C represents the arrangement most likely to minimize the steric effects of the entering alkene. The results are clearly in favor of direction C, which accounts for 90.7% of the final product, whereas direction A is only responsible for 5.9% of it. It is thus apparent that steric repulsions of the olefin are more relevant than the torsion around the copper–carbene axis. The system prefers to pay the penalty of distorting the copper–carbene dihedral angle in order to obtain a less-repulsive path for the incoming olefin.

 © 2008 Wiley-VCH Verlag GmbH & Co. KGaA, Weinheim

Origin of Enantioselectivity

We will analyze here the structure of the maximum energy points in the favored reaction paths to gain some knowledge on the origin of the enantioselectivity. It must first be noted that one path occupies a dominant position, and it is responsible for about 88% of the product formation. This path is C–*S*, and its maximum energy point is located 6.2 kcal/mol above that of the reactants. This barrier is quite low, which thus accounts for the very fast reaction step. It is furthermore well separated from the second-lowest barrier (7.9 kcal/mol, for path A′+*R*), which explains its dominant position. The structure of the maximum energy point for the preferred path C–*S* is displayed in Figure 6. The C–C distances of the bonds being formed are 3.2 Å. It is quite early in the reaction coordinate, but it is near the overall average for all paths shown in Table 1. Because of the C label, the position of the carbene group with respect to the copper substituents is far from optimal, and the computed N–Cu–C_{carb}–$C_{carboxy}$ dihedral angle of –34° is far from the ideal value of –90°, which corresponds to a staggered arrangement, However, the bulky groups are optimally arranged. This can be seen by analyzing the four quadrants in the scheme included in Figure 6. The adamantyl groups of the bis(oxazoline) are in the upper-left and lower-right quadrants. The carboxymethyl substituent of the carbene is in the lower-left quadrant. The bulky phenyl substituents of the olefin are between the two upper quadrants, but definitely far away from the adamantyl group. The potential steric repulsions are thus minimized, and the bulky groups are well distributed in each of the four quadrants. It is interesting to compare the barrier for this path with others sharing the same label C. The C′–*S* path differs in the sense of approach of the olefin, which in this case comes from above the bis(oxazoline) plane on the same side of the carboxymethyl substituent; this creates steric repulsion and a higher barrier of 8.7 kcal/mol. The C–*R* path (barrier of 14.1 kcal/mol) differs from C–*S* in the arrangement of the phenyl substituents of the alkene. Whereas in C–*S* they are on the side of the metal (Cu–C_{carb}–C_H–C_{Ph} 56°), in C–*R* they are away from it (Cu–C_{carb}–C_H–C_{Ph} 168°). The large difference (more than 7 kcal/mol) between both paths suggests a strong electronic preference for the arrangement with the phenyl substituents pointing towards the copper atom. Comparison between the C–*S* (6.2 kcal/mol) and C+*S* (8.7 kcal/mol) paths, indicates a significant electronic preference for the arrangement of the carboxymethyl group with the methoxy substituent pointing towards the entering olefin.

The second-lowest barrier corresponds to path A′+*R*. This path is the most favorable leading to the *R* enantiomer, though only 5.1% of the reactive paths cross it. The highest energy point is portrayed in Figure 7. It is quite early in the reaction coordinate, and the C–C distance is 4.2 Å. It shares a number of features with the maximum energy point for C–*S* discussed above. In particular, the phenyl substituents are oriented towards the metal center, the Cu–C_{carb}–C_H–C_{Ph} dihedral angle is –48°, and the olefin approaches the

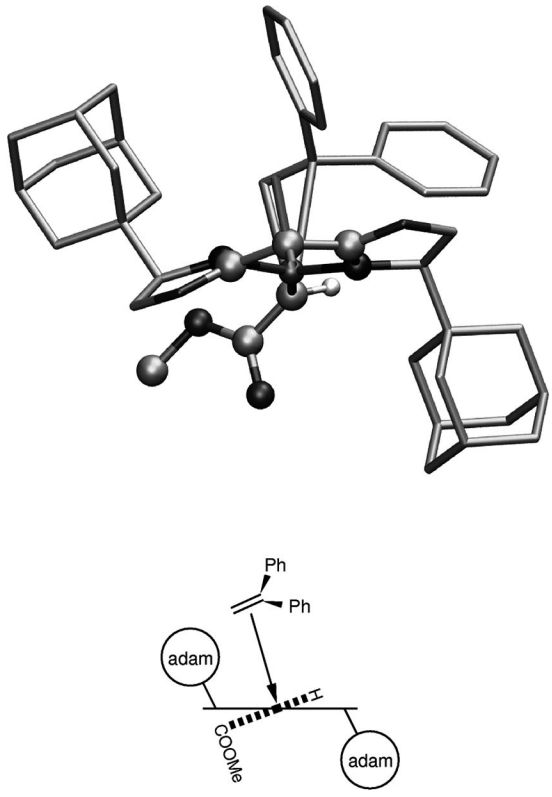

Figure 6. Structure of the transition state corresponding to the most favorable attack, C–*S*; the hydrogen atoms not attached to the carbene are removed for clarity.

carbene from the methoxy side, the O_{Me}–$C_{carboxy}$–C_{carb}–C_H dihedral angle is 50.1°. The main difference, however, resides in the orientation of the carbene plane with respect to the bis(oxazoline) plane. This path has a label A, and the N–Cu–C_{carb}–$C_{carboxy}$ dihedral angle is close to 90°, specifically 97°. This causes the olefin to approach the carbene from a position closer to the bis(oxazoline) plane, and this has an energy penalty that makes this structure less stable than that obtained from the C–*S* path. However, it is still the best possible arrangement between the paths in the A and B directions, as both the ester and the olefin substituents are far from the adamantyl groups, and this is why it is the second-most-favored path.

The structure of the maximum energy point of the third-most-favorable path, B–*S*, is also worthy of comment. It only contributes 2.4% to the final product, but it is a representative example of the conformational complexity of the system. This structure, shown in Figure 8, as corresponds to its B label, has the olefin close to the adamantyl group. As a result, there is a significant deformation of the catalyst that takes place in its most flexible centers, the sp^3 carbon bridge and the copper atom. The adamantyl group in the upper-left quadrant moves forward away from the entering olefin, and as a result, the bis(oxazoline) ring moves upwards from the N–Cu–N plane. This movement is accompanied by a similar movement of the second adamantyl group on the right in Figure 8. The net result is that the central ring of the bis(oxazoline) ligand ends up in a boat-

 © 2008 Wiley-VCH Verlag GmbH & Co. KGaA, Weinheim

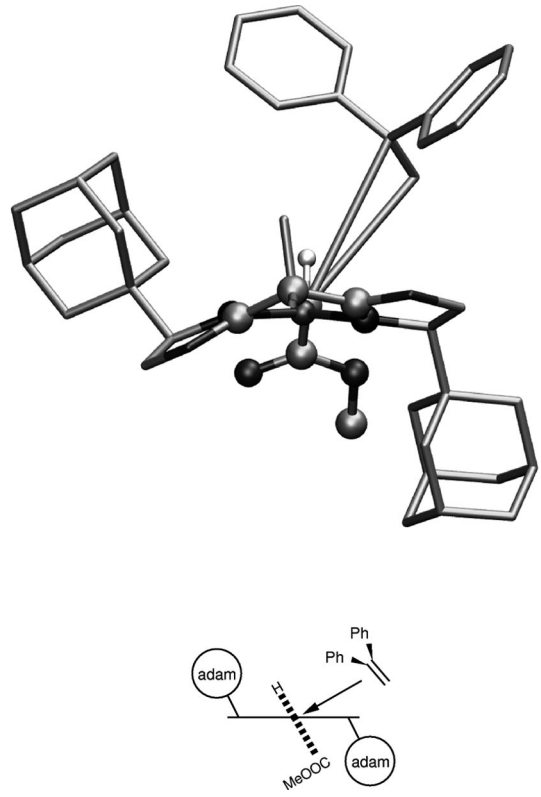

Figure 7. Structure of the transition state corresponding to the most favorable attack leading to the *R* enantiomer, A′+*R*; the hydrogen atoms not attached to the carbene are removed for clarity.

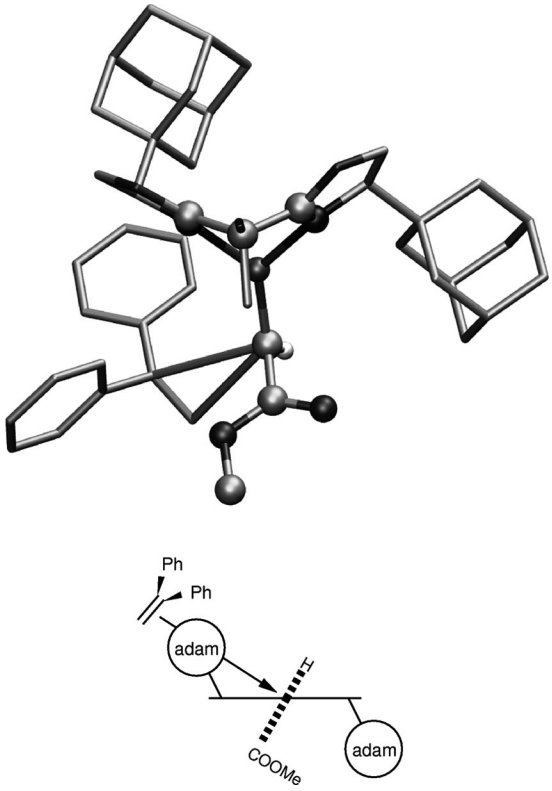

Figure 8. Structure of the transition state corresponding to the third-most-favorable attack, B–*S*; hydrogen atoms not attached to the carbene are removed for clarity.

like conformation. This conformation is preferred over the chair conformation owing to the presence of the olefin partially bound to the carbene.

Conclusions

DFT calculations with the B3LYP functional in a model system confirm that the key step in determining the enantioselectivity of the cyclopropanation of olefins by copper bis(oxazoline) catalysts lacks a transition state in the potential-energy surface. The reaction has a barrier in the Gibbs free-energy surface that is mostly associated to the entropic term. The existence of a barrier explains the experimental observation of enantioselectivity, and the low value (ca. 6 kcal/mol) is compatible with the reaction being fast, occurring at room temperature and below. The two energy surfaces are essentially synchronous, as there is simultaneous approach of the two olefin carbon atoms to the carbene center. We used this synchronicity to define the possible reaction paths in the Gibbs free-energy surface.

ONIOM(B3LYP:UFF) calculations on the reaction of diphenylethylene with [Cu(adam-box)($CHCO_2Me$)] allow the Gibbs free-energy barriers leading to the *R* and *S* products to be estimated. The statistical thermodynamics approaches available in the Gaussian98 program for estimation of the entropic corrections are certainly of limited accuracy, but they allowed the experimental trends to be reproduced. The computed enantiomeric ratio is heavily in favor of the *S* product, which is in good agreement with experiment. The overall enantioselectivity depends on the balance of several different contributions: the relative orientation of the carbene and bis(oxazoline) planes, the steric repulsion between the ester and adamantyl substituents, and the steric repulsion between the olefin phenyl substituents and both the adamantyl groups and the bis(oxazoline) system.

Computational Methods

B3LYP and ONIOM(B3LYP:UFF) calculations were carried out with the Gaussian98 package.[52] ONIOM calculations[53,54] were carried out on the system [Cu(adam-box)($CHCO_2Me$)] plus $Ph_2C{=}CH_2$, which corresponds exactly to the experimental system except for the replacement by methyl of the ethyl substituent of the ester. The QM region consists of [Cu(NH–CH–CH_2–CH–NH)($CHCO_2Me$)] plus $CH_2{=}CH_2$, which was also used as a model system in preliminary DFT calculations. The QM description consisted of the B3LYP functional.[55–57] The LANL2DZ effective core potential was used for copper atoms,[58] and the basis set was 6-31G(d) for nitrogen and carbonyl oxygen atoms and carbene and olefinic carbon atoms;[59] 6-31G was use for the rest of the atoms.[60] The force field for the MM calculations was UFF.[61] This type of computational approach was proved valid recently in an extensive comparison of B3LYP and ONIOM(B3LYP:UFF) calculations for similar systems by García and coworkers.[48] The use of ethylene as QM region from styrene introduced some bias in the philicity of the two carbon atoms, but this was found to be unimportant in previous computational work on styrene dihydroxylation.[62]

 © 2008 Wiley-VCH Verlag GmbH & Co. KGaA, Weinheim

Gibbs free-energy corrections were obtained for selected geometries by using the standard algorithms on the basis of statistical thermodynamics, available in the Gaussian98 program. The Hessians were unprojected. We are aware that these approaches are only exact for stationary points, but we consider that they are still valid to give a reasonable approach to what the real Gibbs free-energy correction would be. Reaction paths were defined by a synchronous approach in the potential-energy surface, with only two bond lengths frozen; the rest of the geometrical parameters were fully optimized for each point in the path. The paths were defined by variations of the C–C distances of the bond being formed from 4.2 to 2.0 Å with a step of 0.2 Å. The barriers for each reaction path were obtained from the Gibbs free energy of its highest point. The barriers were then converted into enantiomeric ratios through the usual approach based on the Maxwell–Boltzmann distribution.[38]

Acknowledgments

Financial support from the Institut Català d'Investigació Química (ICIQ) foundation from the Spanish Ministerio de Ciencia e Innovación through Projects CTQ2005-04968-CO1-01, CTQ2005-09000-CO1-01, CTQ2005-09000-CO1-02, Consolider Ingenio 2010 grants CSD2006-003, and CSD2007-00006 and from the Catalan Direcció General de Recerca through projects 2005SGR00305, 2005SGR00715, and 2005SGR00896.

[1] A. de Meijere, *Chem. Rev.* **2003**, *103*, 931–932.
[2] R. E. Taylor, F. C. Engelhardt, M. J. Schmitt, *Tetrahedron* **2003**, *59*, 5623–5634.
[3] A. J. DelMonte, D. E. Dowdy, D. J. Watson, *Top. Organomet. Chem.* **2004**, *6*, 97–122.
[4] M. Rubin, M. Rubina, V. Gevorgyan, *Chem. Rev.* **2007**, *107*, 3117–3179.
[5] R. Faust, *Angew. Chem. Int. Ed.* **2001**, *40*, 2251–2253.
[6] J. Pietruszka, *Chem. Rev.* **2003**, *103*, 1051–1070.
[7] F. Gnad, O. Reiser, *Chem. Rev.* **2003**, *103*, 1603.
[8] J. Jaffart, M. Etienne, M. Reinhold, J. E. McGrady, F. Maseras, *Chem. Commun.* **2003**, 876–877.
[9] A. de Meijere, S. I. Kozhushkov, H. Schill, *Chem. Rev.* **2006**, *106*, 4926–4996.
[10] A. Reichelt, S. Martin, *Acc. Chem. Res.* **2006**, *39*, 433–442.
[11] M. Fedoryński, *Chem. Rev.* **2003**, *103*, 1099–1132.
[12] H. Reissig, R. Zimmer, *Chem. Rev.* **2003**, *103*, 1151–1196.
[13] H. Lebel, J. Marcoux, C. Molinaro, A. B. Charette, *Chem. Rev.* **2003**, *103*, 977–1050.
[14] E. Díez-Barra, J. M. Fraile, J. I. García, E. García-Verdugo, C. I. Herrerías, S. V. Luis, J. A. Mayoral, P. Sánchez-Verdú, J. Tolosa, *Tetrahedron: Asymmetry* **2003**, *14*, 773–778.
[15] G. Maas, *Chem. Soc. Rev.* **2004**, *33*, 183–190.
[16] P. Müller, S. Grass, S. P. Shahi, G. Bernardinelli, *Tetrahedron* **2004**, *60*, 4755–4763.
[17] M. Cheeseman, F. J. P. Feuillet, A. L. Johnson, S. D. Bull, *Chem. Commun.* **2005**, 2372–2374.
[18] V. Capriati, S. Florio, R. Luisi, F. M. Perna, J. Barluenga, *J. Org. Chem.* **2005**, *70*, 5852–5858.
[19] D. A. Evans, K. A. Woerpel, M. M. Hinman, M. M. Faul, *J. Am. Chem. Soc.* **1991**, *113*, 726–728.
[20] A. K. Ghosh, M. Packiarajan, J. Cappiello, *Tetrahedron: Asymmetry* **1998**, *9*, 1–45.
[21] A. Mandoli, S. Orlandi, D. Pini, P. Salvadori, *Chem. Commun.* **2003**, 2466–2467.
[22] M. B. France, A. K. Milojevich, T. A. Stitt, A. J. Kim, *Tetrahedron Lett.* **2003**, *44*, 9287–9290.
[23] J. G. Knight, P. E. Belcher, *Tetrahedron: Asymmetry* **2005**, *16*, 1415–1418.
[24] E. Carreiro, S. Chercheja, A. J. Burke, J. P. P. Ramalho, A. I. Rodrigues, *J. Mol. Catal. A* **2005**, *236*, 38–45.
[25] M. Itagaki, K. Matsumoto, K. Suenobu, Y. Yamamoto, *Org. Proc. Res. Devel.* **2006**, *10*, 245–250.
[26] J. Werner, C. I. Herrerías, M. Glos, A. Gissibl, M. Fraile, I. Pérez, J. A. Mayoral, O. Reiser, *Adv. Synth. Catal.* **2006**, *348*, 125–132.
[27] T. Portada, M. Roje, Z. Raza, V. Caplar, M. Zinic, V. Sunjic, *Eur. J. Org. Chem.* **2007**, 838–856.
[28] D. E. Bergbreiter, J. H. Tian, *Tetrahedron Lett.* **2007**, *48*, 4499–4503.
[29] C. Bolm, *Angew. Chem. Int. Ed. Engl.* **1991**, *30*, 542–543.
[30] G. Desimoni, G. Faita, K. A. Jorgensen, *Chem. Rev.* **2006**, *106*, 3561–3651.
[31] J. Clariana, J. Comelles, M. Moreno-Mañas, A. Vallribera, *Tetrahedron: Asymmetry* **2002**, *13*, 1551–1554.
[32] J. Comelles, M. Moreno-Mañas, E. Pérez, A. Roglans, R. M. Sebastián, A. Vallribera, *J. Org. Chem.* **2004**, *69*, 6834–6842.
[33] J. Comelles, A. Pericàs, M. Moreno-Mañas, A. Vallribera, G. Drudis-Solé, A. Lledós, T. Parella, A. Roglans, S. García-Granda, L. Roces-Fernández, *J. Org. Chem.* **2007**, *72*, 2077–2087.
[34] F. Maseras, A. Lledós, *Computational Modeling of Homogeneous Catalysis*, Kluwer, Dordrecht, **2002**.
[35] F. Maseras, *Chem. Commun.* **2000**, 1821–1827.
[36] D. Balcells, G. Drudis-Solé, M. Besora, N. Dölker, G. Ujaque, F. Maseras, A. Lledós, *J. Chem. Soc. Faraday Trans.* **2003**, *124*, 429–441.
[37] G. Ujaque, F. Maseras, *Struct. Bonding (Berlin)* **2004**, *112*, 117–149.
[38] D. Balcells, F. Maseras, *New J. Chem.* **2007**, *31*, 333–343.
[39] G. Drudis-Solé, G. Ujaque, F. Maseras, A. Lledós, *Chem. Eur. J.* **2005**, *11*, 1017–1029.
[40] T. Rasmussen, J. F. Jensen, N. Østergaard, D. Tanner, T. Ziegler, P.-O. Norrby, *Chem. Eur. J.* **2002**, *8*, 177–184.
[41] B. F. Straub, *J. Am. Chem. Soc.* **2002**, *124*, 14195–14201.
[42] B. F. Straub, I. Gruber, F. Rominger, P. Hofmann, *J. Organomet. Chem.* **2003**, *684*, 124–143.
[43] D. T. Nowlan, T. M. Gregg, H. M. L. Davies, D. A. Singleton, *J. Am. Chem. Soc.* **2003**, *125*, 15902–15911.
[44] J. M. Fraile, J. I. García, M. J. Gil, V. Martínez-Merino, J. A. Mayoral, L. Salvatella, *J. Am. Chem. Soc.* **2001**, *123*, 7616–7625.
[45] A. Cornejo, J. M. Fraile, J. I. García, M. J. Gil, V. Martínez-Merino, J. A. Mayoral, L. Salvatella, *Organometallics* **2005**, *24*, 3448–3457.
[46] A. Cornejo, J. M. Fraile, J. I. García, M. J. Gil, V. Martínez-Merino, J. A. Mayoral, L. Salvatella, *Angew. Chem. Int. Ed.* **2005**, *44*, 458–461.
[47] J. M. Fraile, J. I. García, M. J. Gil, V. Martínez-Merino, J. A. Mayoral, L. Salvatella, *Chem. Eur. J.* **2004**, *10*, 758–765.
[48] J. I. García, G. Jiménez-Osés, V. Martínez-Merino, J. A. Mayoral, E. Pires, I. Villalba, *Chem. Eur. J.* **2007**, *13*, 4064–4073.
[49] J. M. Fraile, J. I. García, A. Gissibl, J. A. Mayoral, E. Pires, O. Reiser, M. Roldán, I. Villalba, *Chem. Eur. J.* **2007**, *13*, 4064–4073.
[50] K. N. Houk, N. G. Rondan, *J. Am. Chem. Soc.* **1984**, *106*, 4293–4294.
[51] A. A. C. Braga, F. Maseras, J. Urbano, A. Caballero, M. M. Díaz-Requejo, P. J. Pérez, *Organometallics* **2006**, *25*, 5292–5300.
[52] M. J. Frisch, G. W. Trucks, H. B. Schlegel, G. E. Scuseria, M. A. Robb, J. R. Cheeseman, V. G. Zakrzewski, J. A. Montgomery Jr., R. E. Stratmann, J. C. Burant, S. Dapprich, J. M. Millam, A. D. Daniels, K. N. Kudin, M. C. Strain, O. Farkas, J. Tomasi, V. Barone, M. Cossi, R. Cammi, B. Mennucci, C. Pomelli, C. Adamo, S. Clifford, J. Ochterski, G. A. Petersson, P. Y. Ayala, Q. Cui, K. Morokuma, D. K. Malick, A. D. Rabuck, K. Raghavachari, J. B. Foresman, J. Cioslowski, J. V. Ortiz, A. G. Baboul, B. B. Stefanov, G. Liu, A. Liashenko, P. Piskorz, I. Komaromi, R. Gomperts, R. L. Martin, D. J. Fox, T.

 © 2008 Wiley-VCH Verlag GmbH & Co. KGaA, Weinheim

Keith, M. A. Al-Laham, C. Y. Peng, A. Nanayakkara, M. Challacombe, P. M. W. Gill, B. Johnson, W. Chen, M. W. Wong, J. L. Andres, C. Gonzalez, M. Head-Gordon, E. S. Replogle, J. A. Pople, *Gaussian*, Gaussian Inc., Pittsburgh, PA, **1998**.
[53] F. Maseras, K. Morokuma, *J. Comput. Chem.* **1995**, *16*, 1170–1179.
[54] S. Dapprich, I. Komáromi, K. S. Byun, K. Morokuma, M. J. Frisch, *THEOCHEM* **1999**, *461–462*, 1–21.
[55] A. D. Becke, *J. Chem. Phys.* **1993**, *98*, 5648–5652.
[56] C. T. Lee, R. G. Parr, W. Yang, *Phys. Rev. B* **1988**, *37*, 785–789.
[57] P. J. Stephens, F. J. Devlin, C. F. Chabalowski, M. J. Frisch, *J. Phys. Chem.* **1994**, *98*, 11623–11627.
[58] P. J. Hay, W. R. Wadt, *J. Chem. Phys.* **1985**, *82*, 299–310.
[59] M. M. Francl, W. J. Pietro, W. J. Hehre, J. S. Binkley, M. S. Gordon, D. J. Defrees, J. A. Pople, *J. Chem. Phys.* **1982**, *77*, 3654–3665.
[60] W. J. Hehre, R. Ditchfield, J. A. Pople, *J. Chem. Phys.* **1972**, *56*, 2257–2261.
[61] A. K. Rappé, C. J. Casewit, K. S. Colwell, W. A. Goddard, W. M. Skiff, *J. Am. Chem. Soc.* **1992**, *114*, 10024–10035.
[62] G. Ujaque, F. Maseras, A. Lledós, *J. Am. Chem. Soc.* **1999**, *121*, 1317–1323.

Received: August 1, 2008
Published Online: October 10, 2008

 © 2008 Wiley-VCH Verlag GmbH & Co. KGaA, Weinheim